Applied Surface Science 523 (2020) 146503

Contents lists available at ScienceDirect

Applied Surface Science

journal homepage: www.elsevier.com/locate/apsusc

Mxene nanosheets as an emerging solid lubricant for machine elements – Towards increased energy efficiency and service life

Max Marian[a,*], Stephan Tremmel[a], Sandro Wartzack[a], Guichen Song[b], Bo Wang[b], Jinhong Yu[b], Andreas Rosenkranz[c,*]

[a] Engineering Design, Friedrich-Alexander-Universität Erlangen-Nürnberg (FAU), Erlangen, Germany
[b] Key Laboratory of Marine New Materials and Related Technology, Zhejiang Key Laboratory of Marine Materials and Protection Technology, Ningbo Institute of Material Technology & Engineering, Chinese Academy of Sciences, Ningbo 315201, People's Republic of China
[c] Department of Chemical Engineering, Biotechnology and Materials, FCFM, Universidad de Chile, Santiago, Chile

ARTICLE INFO

Keywords:
2D materials
$Ti_3C_2T_x$-nanosheets
Solid lubricants
Machine elements
Thrust ball bearing

ABSTRACT

Solid lubricants like carbon-based materials, transition metal dichalcogenide compounds, polymers and soft metals, each with their specific merits and limitations, pursue the goal of reducing friction and wear between two rubbing surfaces under substantially dry conditions. Newly emerging early transition metal carbides and carbonitrides, such as $Ti_3C_2T_x$-nanosheets (MXenes), seem to be a promising candidate to be used as a solid lubricant due to their weakly bonded multilayer structure with self-lubricating character. For the first time, this paper aims at addressing the application of MXene nanosheets in higher loaded rolling-sliding contacts of machine elements by investigating their friction and wear behavior in thrust ball bearings under ambient conditions. Thereby, a reduction of the frictional torque by a factor of up to 3.2, an extension of the service life by about 2.1 times and a decrease of the linear cumulative wear rate by up to 2.9 compared to uncoated references have been verified. Thus, the $Ti_3C_2T_x$-coating already featured results comparable to reports on graphene, amorphous carbon coatings or advanced transition metal dichalcogenide, which demonstrates the tremendous potential of MXene nanosheets as outstanding, next-generation solid lubricant in machine elements.

1. Introduction

Machine elements such as rolling bearings are usually operated with mineral or synthetic oils to reduce friction and wear. In various applications, however, bearings cannot be conventionally lubricated due to legal and environmental restrictions or physical limitations. Examples are applications in food, textile, paper or medical industry as well as limitations due to ultra-clean conditions, extreme temperatures, radiation or vacuum. To avoid associated premature failures, solid lubricants gain more and more attention due to the possibility to maintain essential lubrication properties. Historically, there have been four distinct classes of solid lubricant materials applied as thin films or coatings, namely carbon-based materials, transition metal dichalcogenide (TMD) compounds, polymers and soft metals [1].

Graphite with its hexagonal lattice and easy-to-shear basal planes by intracrystalline slip due to low surface energies and little adhesion as well as demands moisture or adsorbed gases to passivate the covalent bonds and edges of the basal planes to maintain low friction [2]. Thus, its use in dry environments, particularly in vacuum, is limited [3]. This drawback can be partly overcome by its special form as graphene [4]. There are numerous studies on lower loaded sliding contacts at the nano- [5,6] and micro-scale [4,7–9] thus verifying the excellent frictional performance at favorable ambient conditions. However, only few studies regarding its usage in higher loaded rolling-sliding contacts in macro-scale systems similar as machine components such as rolling element bearings can be found [10]. The most common usage of graphite is in metal- and polymer-matrix self-lubricating composites or, partially, as a loose or resin-bonded coating [1].

While initial studies on molybdenum disulphide (MoS_2), as an example for TMD compounds, were mainly driven by space exploration [11,12], recent studies were rather ecologically motivated [13–15]. The tribological properties of MoS_2 as a solid lubricant have been extensively analyzed for sliding contacts, while there are fewer studies when used in rolling contact conditions [16,17]. Despite the improvement of tribological properties due to its hexagonal crystal structure and the low coefficient of friction (*COF*) due to the ease of its basal

* Corresponding authors.
E-mail addresses: marian@mfk.fau.de (M. Marian), tremmel@mfk.fau.de (S. Tremmel), wartzack@mfk.fau.de (S. Wartzack), songguichen@nimte.ac.cn (G. Song), wangb@nimte.ac.cn (B. Wang), yujinhong@nimte.ac.cn (J. Yu), arosenkranz@ing.uchile.cl (A. Rosenkranz).

https://doi.org/10.1016/j.apsusc.2020.146503
Received 9 March 2020; Accepted 24 April 2020
Available online 29 April 2020

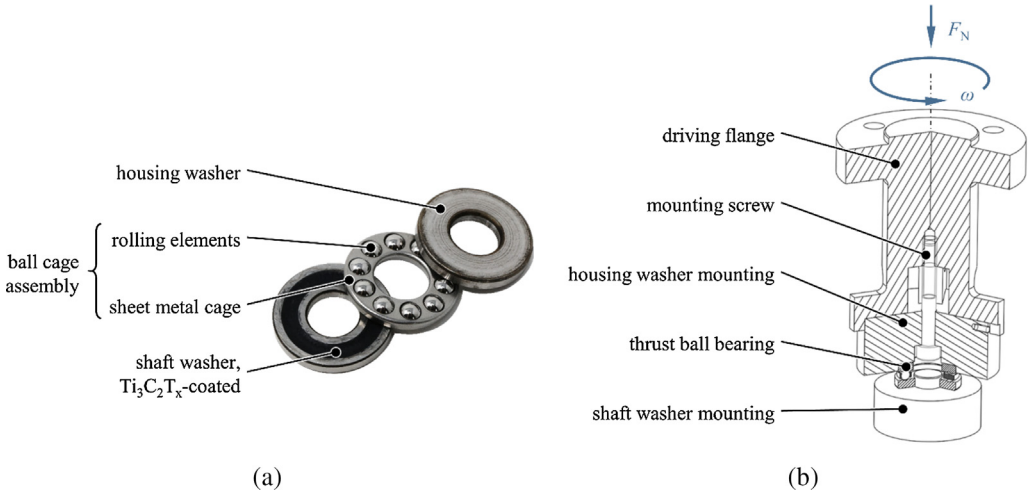

Fig. 1. Housing washer, ball cage assembly and exemplarily $Ti_3C_2T_x$-coated shaft washer of a thrust ball bearing 51201 (a) and set-up within the tribometer for service life testing (b).

plane shearing especially under vacuum conditions, MoS_2 is susceptible to ambient air with humidity due to oxidation [18–21]. Overall, the achievable revolutions/overrollings until end of the service life of rolling bearings vary depending on the coating system applied, the number of coated components, the load and, in particular, the ambient medium [22].

Among polymeric materials, polytetrafluoroethylene (PTFE) is well known for its low friction performance due to its little intermolecular cohesion [23]. This holds true in vacuum and atmosphere due to its low chemical reactivity [3]. However, pure PTFE suffers from a poor wear resistance and limited load carrying capacity, which can be partially improved by the addition of suitable fillers [3,24]. Moreover, the low thermal inertia of PTFE inhibits heat dissipation, resulting in premature failure due to melting and limiting usage rather to low-speed sliding applications [3].

Metals, such as gold, silver, indium, tin or lead and corresponding alloys, possess low friction when being applied as a coating on relatively hard substrates. Typically, soft metal film lubrication occurs by shear within the coating rather than by surface transfer, resulting in significantly higher friction compared to other solid lubricants [1]. Therefore, it is particularly useful in rolling and non-sliding applications and most relevant at higher temperatures and under vacuum [25]. For example, silver and barium films have been successfully used in lightly loaded ball bearings in high X-ray tubes, while silver and gold films have been successfully tested for usage in spacecraft [26,27].

This brief summary on existing well-established solid lubricants makes evident that they have been extensively studied in fundamental, model tribological test-rigs under various operating conditions. However, their usage in applied machine components under more realistic working conditions is still scarce. Moreover, it becomes obvious that the aforementioned solid lubricants have all their respective limitations and short-comings, which directly ask for more research in this direction as well as new, more advanced solid lubricant systems.

In the last 5 years, early transition metal carbides and/or carbonitrides based upon MAX-phases and named as MXenes as introduced by Naguib et al. [28] have experienced considerable attention in the fields of energy storage and catalysis due to their outstanding material's properties. Their main process route is to remove the A layers of $M_{n+1}AX_n$ (M: early transition metal, A: group IIIA or IVA element and X: C or N with n = 1, 2 or 3) by selective etching [28,29]. Besides energetic and catalytic applications, MXenes are particularly interesting for tribological purposes due to their graphite-like structure, low shear strength and self-lubrication ability [30], which has already been verified by density functional calculations and molecular dynamic simulations [31].

Although bearing tremendous potential, the use of MXenes for tribological purposes is still very scarce [32–38]. Lian et al. [30] applied a Ti_3C_2-film with a thickness of 200 nm on copper disks by spray coating and verified a 3-fold friction as well as a 10-fold wear reduction in ball-on-disk experiments. Rosenkranz et al. [39] studied the frictional performance of thin layers of $Ti_3C_2T_x$-nanosheets drop casted on stainless steel substrates under dry conditions. A pronounced three fold reduction in the *COF* combined with a significant reduction of wear was observed. Guo et al. [40] studied nano-mechanical properties of MXenes using atomic force microscopy as a function of the applied normal force, temperature and pressure. Thereby, better frictional behavior and adhesional properties were observed at higher temperatures and lower applied pressures. Yin et al. investigated MXene and MXene/nanodiamond [41] as well as MXene/graphene quantum dots composite coatings [42] under dry conditions and low contact pressures. For coatings consisting of pure MXenes, they observed stable *COF*s around 0.3 against PTFE and almost no detectable wear, which was traced back to the formation of a wear resistant tribofilm consisting of densified MXene nanoflakes. In case of the MXene/nanodiamond coating or MXene/graphene quantum dots composite coatings, *COF*s of about 0.16 and 0.20 as well as ultralow wear have been detected wear track. A detailed investigation via focussed ion beam and transmission electron microscopy revealed the formation of a nano-structured tribofilm.

Summarizing, MXene nanosheets can be considered as a promising alternative to common solid lubricants, which may overcome some of the aforementioned limitations with the potential use in machine components under a wide range of environmental conditions and realistic working conditions. Therefore, this contribution aims for the first time at investigating the tribological performance of $Ti_3C_2T_x$-nanosheets as a solid lubricant used in higher loaded rolling-sliding contacts of thrust ball bearings to assess their full potential.

2. Materials and methods

2.1. Materials

Commercially available thrust ball bearings 51,201 according to ISO 104 [43] consisting of shaft washer, housing washer and ball cage assembly were used as substrates (Fig. 1a). These were chosen due to their simplicity of the coating's deposition and their high spinning friction as well as high amount of slippage. Prior to deposition and testing, all components were ultrasonically cleaned (BANDELIN, Sonorex Super RK 255H, 160 W, 35 kHz, room temperature) in acetone and isopropyl

alcohol for 10 min each and blow dried using nitrogen.

The initial Ti_3AlC_2-powder was purchased from FORSMAN SCIENTIFIC Co. Ltd., Beijing (China). To synthesize multi-layer $Ti_3C_2T_x$-nanosheets, Ti_3AlC_2-powder (10 g) was immersed in 100 ml of a 40% hydrofluoric acid solution. The mixture was stirred for 24 h at room temperature. The as-prepared suspension was then washed using deionized water several times until reaching a pH above 6 and subsequently centrifuged to separate the powder. Afterwards, the washed powder was filtered under vacuum conditions and then dried at room temperature for 24 h in a vacuum oven.

For deposition, the $Ti_3C_2T_x$-nanosheets were dispersed in acetone with a concentration of 12 mg/ml. Good dispersion was assured by ultrasonication (BANDELIN, Sonorex Super RK 255H, 160 W, 35 kHz, room temperature). Subsequently, to exploit the available volume, 300 µl onto each, shaft and housing washer, as well as 400 µl onto the ball cage assembly were deposited by drop casting using a syringe (Hamilton, 1000 series gastight 81420). Special attention was paid to a rather homogenous distribution of the $Ti_3C_2T_x$-nanosheets after solvent's evaporation.

2.2. Characterization of the $Ti_3C_2T_x$-nanosheets

The number of layers, structure and an overall quality of the MXene nanosheets has been investigated using high-resolution transmission electron microscopy (HR-TEM; FEI, Tecnai F20) with an acceleration voltage of 200 kV. Their chemical composition was analyzed by energy dispersive X-ray spectroscopy (TEM-EDX) using EDAX detector. Information related to their surface chemistry and surface terminations has been gained by Raman spectroscopy, X-Ray photoelectron spectroscopy (XPS) and X-Ray diffraction (XRD). To perform Raman spectroscopy (WITEC, Alpha 300 RA), an excitation wavelength of 633 nm, a grating of 300 g/mm and 10% of the maximum laser intensity were utilized. The spectra were obtained using four seconds of integration time and a total number of 256 accumulations to ensure a sufficiently high signal-to-noise ratio. The MXene nanosheets were examined by XPS (Physical Electronics model 1257) using non-monochromatic MgK_α radiation, operating the source at 15 kV and 400 W. The scans were acquired using a pass energy of 44.75 eV. Narrow scans of the C_{1s}, F_{1s}, O_{1s} and Ti_{2p} regions were recorded using a step size of 0.025 eV. The MULTIPAK package has been used for data processing. Energy correction was performed by assigning 274.8 eV to the maximum of the C_{1s} peak. The Shirley method was used for background subtraction for the C_{1s}, F_{1s}, O_{1s} regions, while linear subtraction was utilized for the Ti_{2p} region. The peaks were fitted with Lorentz Gaussian functions, maintaining the number of curves as low as possible to provide an acceptable match: two singlets for the F_{1s} and O_{1s} regions, three singlets for the C_{1s} region, and three doublets for the Ti_{2p} region. The XRD analysis was done using a powder diffractometer in Bragg-Brentano configuration (PANalytical Empyrean) operating at 40 kV and 40 mA with CuK_α irradiation. The respective angular step size was 0.026° while using a dwell time of 1396.89 s for each measuring point.

2.3. Tribological testing

A tribometer (WAZAU, TRM1000) with a modified setup according to Fig. 1b was used for tribological testing. All tests were carried out under laboratory conditions (temperature ≈ 20 °C, relative humidity ≈ 50%). Frictional torque, normal force and cumulative wear distance were detected on the stationary shaft mounting. The latter was cardanically mounted for uniform load application. The housing washer mounting constantly rotated at 1000 min^{-1}. The applied axial force of 130 N resulted in initial maximum Hertzian pressures of 800 MPa in the ball/raceway-contact. The maximum service life of the bearing has been reached when the measured frictional torque increased to a value of 1.3 Nm due to successive wear. In order to obtain results independent of the number of rolling elements, the amount of overrollings of each volume element of the raceway endured until failure was taken as the reference value for bearing service life and wear rate. Moreover, the chemical composition of the as-deposited as well as the worn $Ti_3C_2T_x$-coatings was analyzed by Raman spectroscopy (HORIBA, LabRAM HR 800). Thereby, an excitation wavelength of 633 nm and 50% of the maximum laser intensity were used. To evaluate failure modes and wear mechanisms, the specimens were subjected to optical analysis using photo documentation (CANON, EOS 70D), digital light microscopy (LEICA, DM4000) and laser scanning microscopy (KEYENCE, VK-X200). Moreover, the masses of the ball cage assemblies were gravimetrically measured (KERN, ALJ 500-4A) prior to and after testing. Prior to ex-situ characterization, the bearing components were ultrasonically cleaned (BANDELIN, Sonorex Super RK 255H, 160 W, 35 kHz, room temperature) in isopropyl alcohol for 10 min.

3. Results and discussion

3.1. Characterization

In order to assess the overall quality of the MXene nanosheets, HR-TEM combined with EDX has been conducted. The regular and homogenous multi-layered nature of the MXene nanosheets with a layer distance of about 820 pm can be well recognized in Fig. 2a and b. The analysis by TEM-EDX (not shown here) revealed that the main elements are titanium, carbon, oxygen and fluorine with only a minor and negligible signal stemming from aluminum (0.3 wt-%). XRD, Raman spectroscopy and XPS have been utilized to fully characterize the respective surface chemistry. The observed diffraction peaks (Fig. 2c) can be clearly correlated with different surface terminations, namely −OH, sbndO and −F groups [44]. The most dominant peak correlated well with hydroxyl (−OH) terminations, followed by weaker −F and −O contributions. The occurrence of these terminations can be explained by the selective etching process to synthesize the MXene nanosheets. During synthesis, the aluminum has been etched by HF and replaced by the observed surface terminations. The presented Raman spectrum (Fig. 2d) confirms the observed surface terminations in XRD, since the spectrum showed pronounced peaks at 125, 212 and 701 cm^{-1} as well as broad peaks around 285, 376 and 600 cm^{-1}. The observed Raman bands can be directly connected with vibrations coming from $Ti_3C_2O_2$, $Ti_3C_2F_2$ and $Ti_3C_2(OH)_2$ [44–46].

Obtained XPS results after the respective peak fitting and background correction are summarized in Table 1. The peak fitting of C_{1s} revealed the main contribution at 284.7 eV (86%), which can be directly correlated to C−C chemical environment and adventitious carbon. The 281.6 eV peak characterizes the contribution of metal carbides and can be associated with C-Ti-T_x [47,48], while the contribution at 286.7 eV mainly matched with hydrocarbons/organic compounds [47,49]. Regarding the O_{1s} peak, the most pronounced contribution (90%) lays at a binding energy of 532.2 eV, which is assigned to hydroxides suggesting −OH terminations. Following the interpretation from Halim et al. [47], this may stand for organic compounds or C-Ti-$(OH)_x$. Having the results of XRD and Raman spectroscopy in mind, the latter seems to be reasonable. A minor contribution (10%) at 529.6 eV is characteristic for TiO_2 [50]. The dominant contribution of F_{1s} (75%) at 685.2 eV can be assigned to fluorinated TiO_2 ($TiO_{2-x}F_x$) [51]. The second F_{1s} contribution (25%) at 687.1 eV can be assigned to fluorine in C_6F_6 (graphite fluorides) [52]. The main contribution of the Ti_{2p} peak (62%) located at 454.9 and 460.1 eV is correlated to titanium carbides (MXenes) [44,49,53]. The second one (17%) at 456.1 and 461.4 eV can be assigned in a general way to Ti^{+2} in a variety of moieties, consisting of titanium bounds to carbon and/or to oxygen or hydroxides such as C-Ti-OH, which matches again with the results of XRD and Raman spectroscopy [44,47]. The last contribution (21%) at 457.8 and 462.7 eV can be assigned to Ti^{+3} and C-Ti-O [44,47], which goes again hand in hand with the results of XRD and Raman spectroscopy.

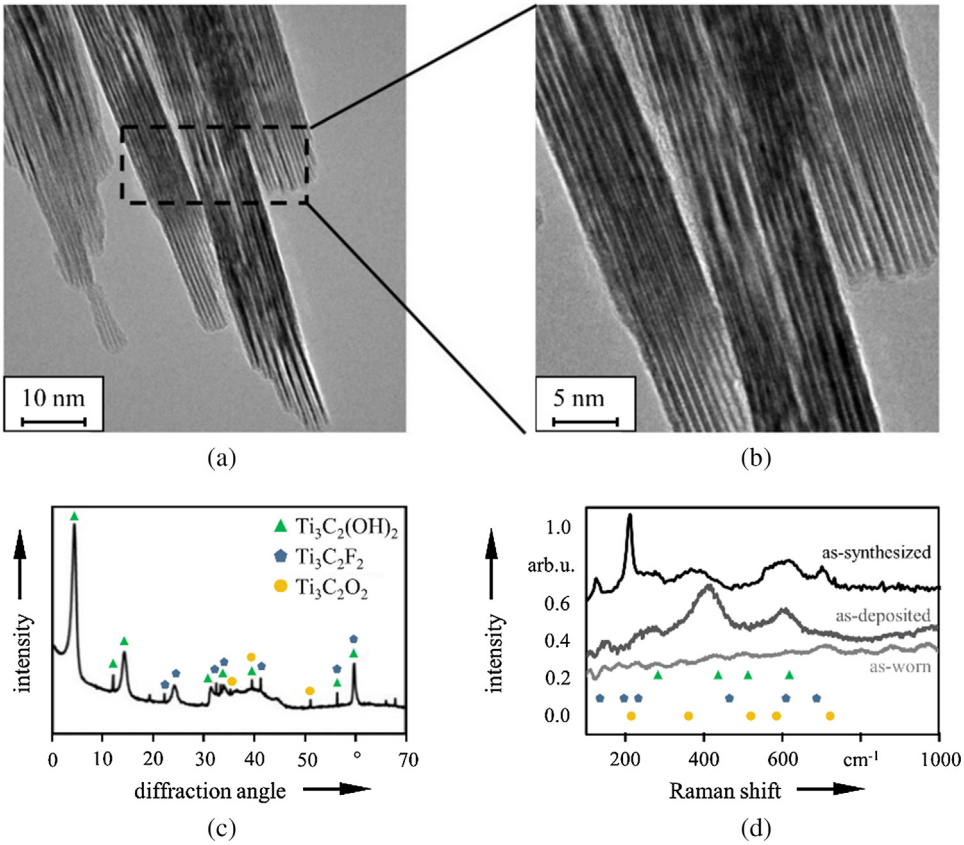

Fig. 2. Characterization of the as-synthesized $Ti_3C_2T_x$-nanosheets by HR-TEM (a and b), XRD (c) and Raman spectroscopy (d).

3.2. Frictional torque and service life

Representative frictional torque curves over time (overrollings) for an uncoated reference and $Ti_3C_2T_x$-coated sample are depicted in Fig. 3a, whereas the averaged values within the first 250 000 overrollings for both types are illustrated in Fig. 3b. The mean number of overrollings until frictional torque reached the termination criterion (service life) is summarized in Fig. 4a, while the averaged mass loss of the ball cage assembly is shown in Fig. 4b. Respective photographic, light microscopic and laser scanning microscopic images of unworn, reference and $Ti_3C_2T_x$-coated bearing components are depicted in Figs. 5–7. Representative cumulative wear distances and averaged linear wear rates for an uncoated reference and $Ti_3C_2T_x$-coated sample are illustrated in Fig. 8a and b, respectively.

For the uncoated reference sample, after a short running-in, the frictional torque reached stable and high levels with strongly pronounced fluctuations (Fig. 3a, grey) due to the lack of lubricant, accompanied by a severe noise development already at the beginning. The mean torque value of the reference samples was about 0.35 Nm (Fig. 3b, grey). After a sudden increase in the frictional torque, the uncoated specimens failed after an average of $436{\cdot}10^3$ overrollings (Fig. 4a, grey). The analysis of the failure causes of the bearing components indicated that the distinct rise in the frictional torque at the end of the test was not due to rolling contact fatigue but rather to massive damage to the sheet metal cage. The severe cage wear resulted from a pronounced cage instability, which was promoted by the lack of damping by a lubricant. The associated orbital and tilting movements of the rolling element guided cage increased stresses acting between balls and cage pockets. When a critical wear condition was reached, clamping, fretting and overheating of the balls in the cage terminated the bearing's service life (Fig. 5c). Even the raceways of the washers already showed strong signs of wear (Fig. 5d, 6b and 7b), with pittings,

Table 1
Summary of the respective peak fitting of the different photoelectron peaks and their characteristics such as binding energy, FWHM, fraction and assignment. The values given in the parenthesis correspond to the $Ti_{2p1/2}$ component. The column "Elemental fraction" is the nominal contribution of each element to the spectrum. Notice that the superficial Ti:C ratio is 1:10, which reflects that the surface composition deviates strongly from the body composition of the nanoparticles. However, no confident quantitative assessment can be provided, since the sample incorporates carbon at the surface after the exposure to the atmosphere.

XPS peak	BE in eV	FWHM	peak fraction in %	elemental fraction in %	Assigment	reference
C_{1s}	284.7	1.8	86	70	C-C, adventitious	[4847,4847,49]
	281.6	1.2	7		Titanium carbide C-Ti-T_x	
	286.7	1.7	7		Hydrocarbons	
$Ti_{2p3/2}$	454.9 (460.1)	1.5 (1.9)	62	7	Titanium carbide (MXene)	[44,49,534444,47]
	456.1 (461.4)	1.8 (1.7)	17		C-Ti-(O or OH)	
	457.8 (462.7)	1.8 (1.8)	21		C-Ti-O	
O_{1s}	532.2	3.0	90	14	C-Ti-$(OH)_x$	[4748,50]
	529.6	1.1	10		TiO_2	
F_{1s}	685.2	1.9	75	9	$TiO_{2-x}F_x$	[51]
	687.1	2.2	25		Graphite fluorides (C_6F_6)	

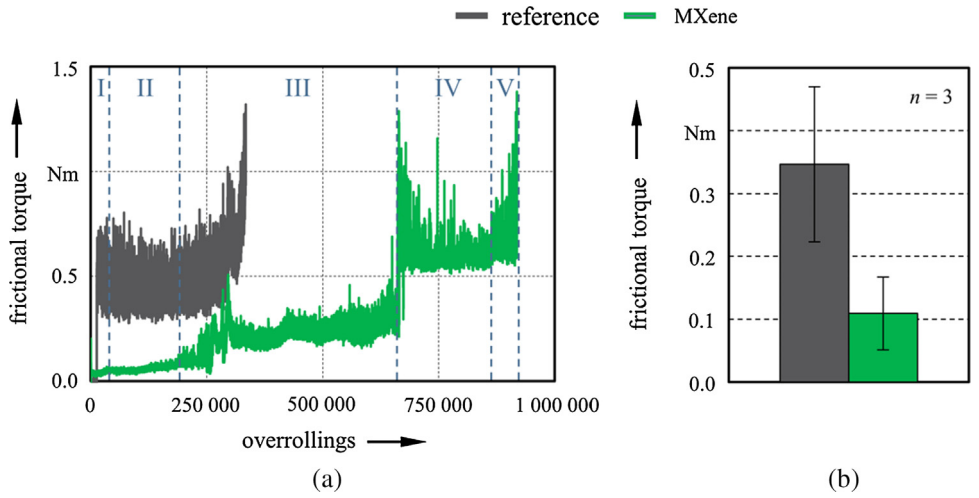

Fig. 3. Representative frictional torque versus overrollings (a) and averaged frictional torque within the first 250 000 overrollings (b) for the reference and $Ti_3C_2T_x$-coated samples.

slip marks and smearing. Thus, comparatively severe wear was already apparent in the middle range of the service life. The cumulative wear increased continuously during operation until dropping abruptly and becoming negative when the bearing failed due to hot running and thermal expansion of the components (Fig. 8a and b, grey).

In contrast, the frictional torque curve of the $Ti_3C_2T_x$-coated bearings can be subdivided into five phases (Fig. 3a, green). After a short running-in phase (I), friction dropped and stabilized at a certain frictional torque. During the operating phase (II), a steady friction level with low fluctuations and averaged values around 0.11 Nm (Fig. 3b, green) was observed. Compared to the uncoated reference, this corresponded to a reduction of frictional torque by a factor of 3.2, which was attributed to the self-lubricating behavior of the MXene nanosheets and the potential formation of a beneficial tribo-film consisting of densified MXene nanosheets [39,41]. At times for which the reference bearings were already threatening to fail, cage, rolling elements and raceways of the $Ti_3C_2T_x$-coated bearings were still well protected against wear (Fig. 4b, blue, Fig. 5e and f, 6c, 7c). This was followed by a transition phase (III) in which friction gradually increased. The latter, in turn, was replaced by a further interim phase (IV), in which the friction increased more strongly and proceeded with stronger fluctuations at the level of the uncoated reference. Finally, clear signs of bearing malfunction were observed in the failure phase (V). Thus, the MXene coated bearings failed on average after approximately $936 \cdot 10^3$ overrollings (Fig. 4, green), an increase by a factor of about 2.1 compared to the reference. It is worth to mention that, despite the early stage of tribological research since the discovery of MXene nanosheets, they have already reached runtimes in dry-running rolling bearing applications achieved with graphene [10], amorphous carbon coatings [54,55] or transition metal dichalcogenide evolved over the last 50 years [22]. Therefore, it may be assumed that further research on MXene nanosheets such as, for instance, optimized synthesis methods leading to tailored functional groups, can further boost the tribological performance thus outperforming the existing state-of-the art solid lubricants. Again, the end of the service life was primarily driven by cage wear (Fig. 5g), resulting in fretting and overheating of the rolling elements within the cage. This is also well reflected in the corresponding mass loss of the ball cage assembly (Fig. 4b). Due to the fatal failure with clamping and hot-running rolling elements, however, further chemical ex-situ analysis of the bearing component was not possible (Fig. 2d). However, the raceways particularly showed fewer signs of wear than reference bearings (Fig. 5h, 6d and 7d) and it is assumed that the $Ti_3C_2T_x$-nanosheetss still had a friction and wear-reducing effect even after this long operating time. This was also reflected in the linear cumulative wear (Fig. 8a, green) and the up to 2.9-fold lower wear rate compared to reference bearings.

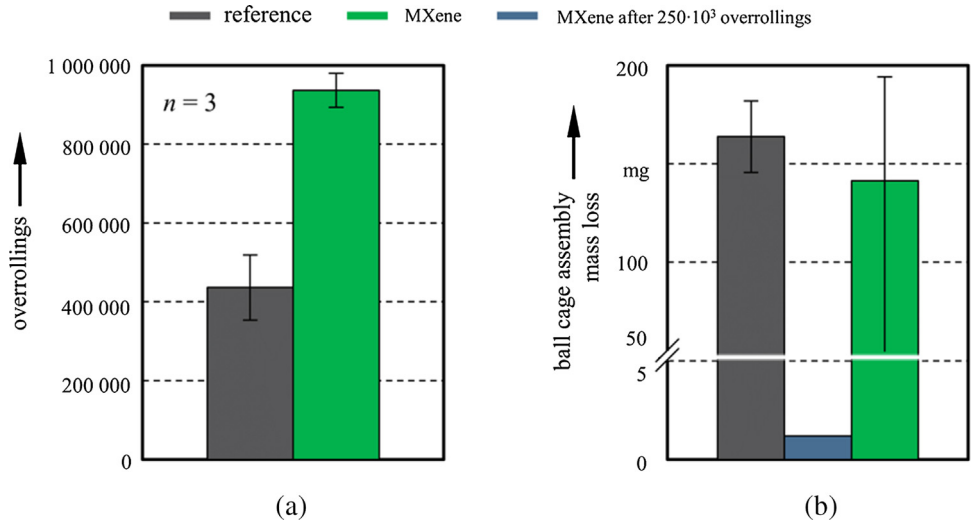

Fig. 4. Averaged service life (a) and mass loss of the ball cage assembly (b) for the reference and $Ti_3C_2T_x$-coated samples.

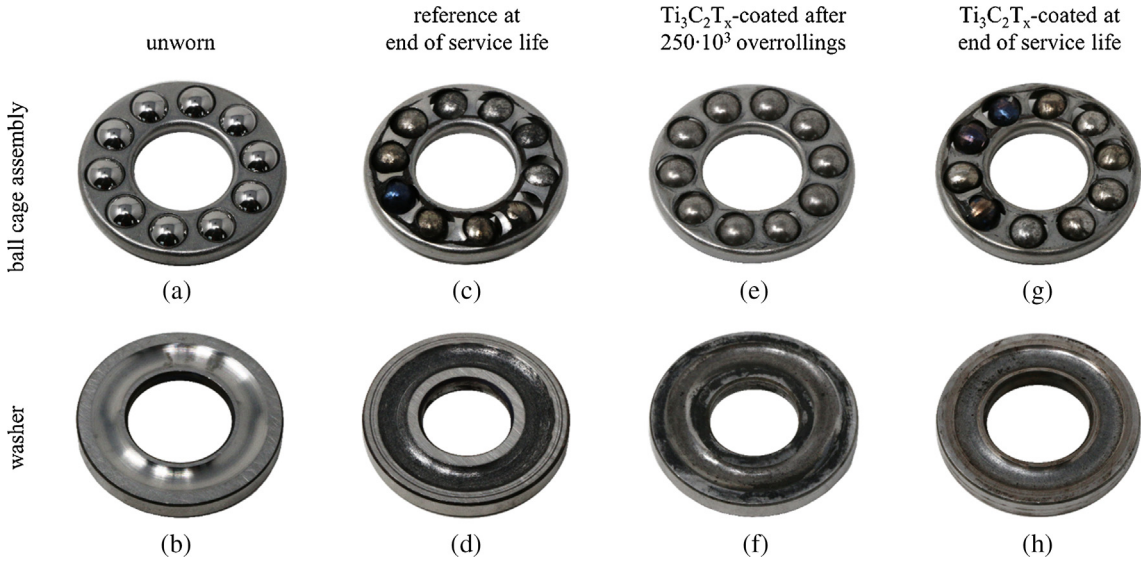

Fig. 5. Photographic images of a ball cage assembly and a washer after bearing failure of an unworn (a, b), a reference at end of service life (c, d), a $Ti_3C_2T_x$-coated sample after 250 000 overrollings (e, f) and at end of service life (g, h).

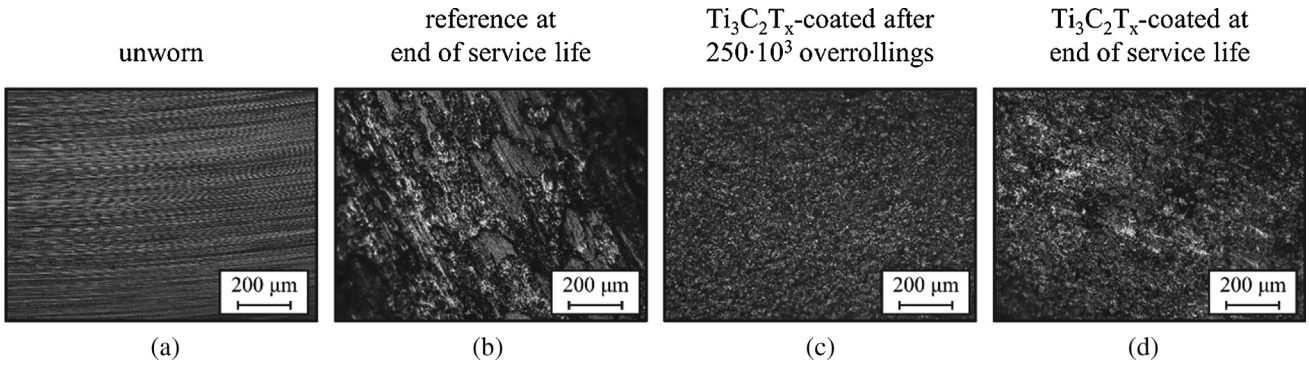

Fig. 6. Light microscopy images of the raceway of an unworn (a), a reference at end of service life (b), a $Ti_3C_2T_x$-coated sample after 250 000 overrollings (c) and at end of service life (d).

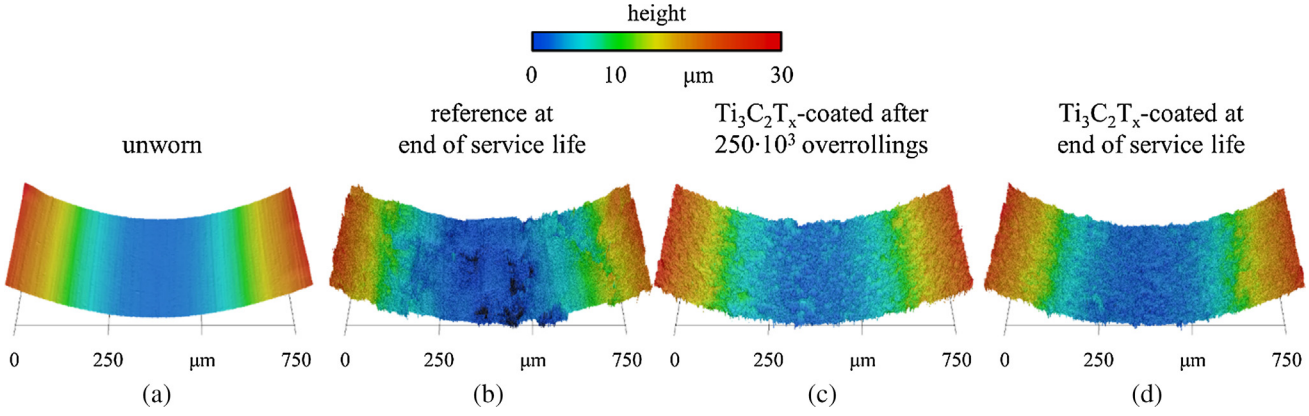

Fig. 7. Laser scanning microscopy images of the raceway of an unworn (a), a reference at end of service life (b), a $Ti_3C_2T_x$-coated sample after 250 000 overrollings (c) and at end of service life (d).

4. Conclusions

For the first time, accurate material characterization and tribological experiments were used to assess the influence of $Ti_3C_2T_x$-nanosheets on energy efficiency and operating time when used as a solid lubricant in higher loaded rolling-sliding contacts of machine elements. Thereby, a reduction of the frictional torque by a factor of up to 3.2, an extension of the service life by about 2.1 times and a decrease of the linear cumulative wear rate by up to 2.9 compared to uncoated references was observed. These results were already comparable to those from various reports in literature on graphene, amorphous carbon coatings or advanced transition metal dichalcogenide. Consequently, this strongly emphasizes the outstanding friction-reducing and wear-protecting properties of MXene nanosheets when applied as solid

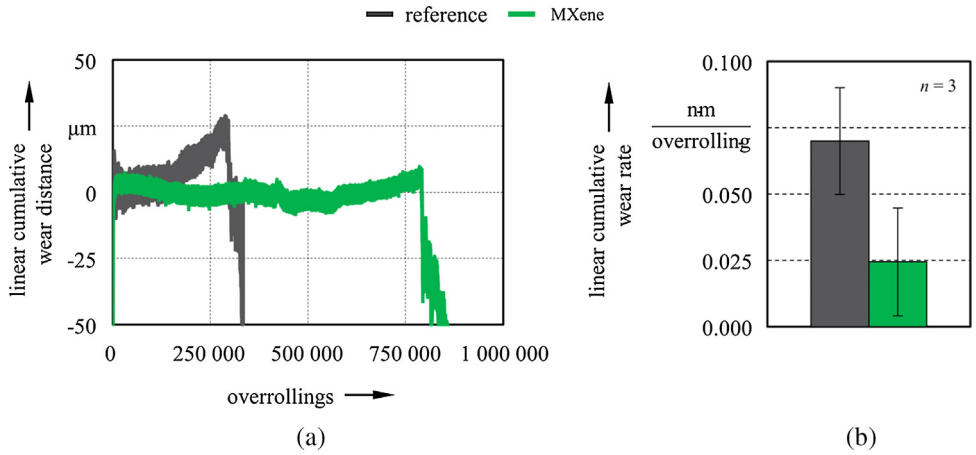

Fig. 8. Representative cumulative wear distance versus overrollings (a) and linear wear rates averaged over the two middle quantiles of service life (b) for the reference and $Ti_3C_2T_x$-coated samples.

lubricants in machine components.

Declaration of Competing Interest

The authors declare that they have no known competing financial interests or personal relationships that could have appeared to influence the work reported in this paper.

Acknowledgments

M. Marian, S. Tremmel and S. Wartzack greatly acknowledge the continuous support of the technical faculty of Friedrich-Alexander-Universität (FAU) Erlangen-Nürnberg, Germany. Student assistant K. Feile from Engineering Design, FAU Erlangen-Nürnberg, Germany is kindly acknowledged for the assistance in tribological testing and ex-situ characterization. A. Rosenkranz kindly acknowledges the help of Prof. Dr. V. M. Fuenzalida and Prof. Dr. R. Espinoza regarding the XPS and HR-TEM measurements, respectively.

Funding

This work was supported by CONICYT, Chile within the project Fondecyt 11180121 as well as the VID of the University of Chile in the framework of “U-Inicia” UI013/2018.

Author Contributions

M. Marian conceived the idea, designed and carried out the experiments and analyzed the data. G. C. Song, B. Wang and J. H. Yu synthesized the MXene samples, which were characterized by A. Rosenkranz. S. Tremmel and S. Wartzack provided suggestions for discussions. M. Marian and A. Rosenkranz wrote the manuscript. All authors have reviewed, edited and thoroughly read the manuscript as well as approved its final version.

Appendix A. Supplementary material

Supplementary data to this article can be found online at https://doi.org/10.1016/j.apsusc.2020.146503.

References

[1] T.W. Scharf, S.V. Prasad, J. Mater. Sci. 48 (2013) 511–531, https://doi.org/10.1007/s10853-012-7038-2.
[2] R.F. Deacon, J.F. Goodman, Proc. R. Soc. Lond. A 243 (1958) 464–482, https://doi.org/10.1098/rspa.1958.0013.
[3] S. Rao, M. Sandeep, R. Kumaraswami, A. Shravan, Int. J. Mech. Eng. Technol. 7 (2016) 193–199.
[4] D. Berman, A. Erdemir, A.V. Sumant, Mater. Today 17 (2014) 31–42, https://doi.org/10.1016/j.mattod.2013.12.003.
[5] L. Xu, T.-B. Ma, Y.-Z. Hu, H. Wang, Nanotechnology 22 (2011) 285708, , https://doi.org/10.1088/0957-4484/22/28/285708.
[6] O. Penkov, H.-J. Kim, H.-J. Kim, D.-E. Kim, Int. J. Precis. Eng. Manuf. 15 (2014) 577–585, https://doi.org/10.1007/s12541-014-0373-2.
[7] D. Berman, A. Erdemir, A.V. Sumant, Carbon 59 (2013) 167–175, https://doi.org/10.1016/j.carbon.2013.03.006.
[8] X. Feng, S. Kwon, J.Y. Park, M. Salmeron, ACS Nano 7 (2013) 1718–1724, https://doi.org/10.1021/nn305722d.
[9] M.-S. Won, O.V. Penkov, D.-E. Kim, Carbon 54 (2013) 472–481, https://doi.org/10.1016/j.carbon.2012.12.007.
[10] F. Pape, G. Poll, Lubricants 8 (2020) 3, https://doi.org/10.3390/lubricants8010003.
[11] T. Spalvins, A S L E Transactions 12 (1969) 36–43, https://doi.org/10.1080/05698196908972244.
[12] M.R. Hilton, P.D. Fleischauer, Surf. Coat. Technol. 54–55 (1992) 435–441, https://doi.org/10.1016/S0257-8972(07)80062-4.
[13] P.D. Fleischauer, R. Bauer, Tribol. Trans. 31 (1988) 239–250, https://doi.org/10.1080/10402008808981819.
[14] M.R. Hilton, R. Bauer, P.D. Fleischauer, International Conference on Metallurgical Coatings, San Diego, 1989 188 (1990) 219–236. DOI: 10.1016/0040-6090(90)90285-L.
[15] I.L. Singer, MRS Proc. 140 (1988) 262, https://doi.org/10.1557/PROC-140-215.
[16] A. Mesgarnejad, M.M. Khonsari, Wear 269 (2010) 547–556, https://doi.org/10.1016/j.wear.2010.05.010.
[17] H. Singh, K.C. Mutyala, H. Mohseni, T.W. Scharf, R.D. Evans, G.L. Doll, Tribol. Trans. 58 (2015) 767–777, https://doi.org/10.1080/10402004.2015.1015758.
[18] B. Vierneusel, T. Schneider, S. Tremmel, S. Wartzack, T. Gradt, Surf. Coat. Technol. 235 (2013) 97–107, https://doi.org/10.1016/j.surfcoat.2013.07.019.
[19] H.S. Khare, D.L. Burris, Tribol. Lett. 52 (2013) 485–493, https://doi.org/10.1007/s11249-013-0233-8.
[20] M. Uemura, K. Saito, K. Nakao, Tribol. Trans. 33 (1990) 551–556, https://doi.org/10.1080/10402009008981988.
[21] R.P. Pardee, A S L E Transactions 15 (1972) 130–142, https://doi.org/10.1080/05698197208981409.
[22] B. Vierneusel, S. Tremmel, S. Wartzack, in: 11. VDI-Fachtagung Gleit- und Wälzlagerungen: Gestaltung, Berechnung, Einsatz, VDI-Verl., Düsseldorf, 6.-7.5., pp. 117–132.
[23] B.J. Briscoe, D. Tabor, Wear 34 (1975) 29–38, https://doi.org/10.1016/0043-1648(75)90306-3.
[24] S. Bahadur, D. Tabor, Wear 98 (1984) 1–13, https://doi.org/10.1016/0043-1648(84)90213-8.
[25] S.H. Wan, Encyclopedia of Tribology, Springer, US, Boston, MA, 2013, pp. 3152–3159.
[26] K. Miyoshi, Solid Lubrication Fundamentals and Applications, Marcel Dekker, New York, 2001.
[27] F.J. Clauss, Solid Lubricants and Self-Lubricating Solids, Academic Press, New York, London, 1972.
[28] M. Naguib, V.N. Mochalin, M.W. Barsoum, Y. Gogotsi, Adv. Mater. (Deerfield Beach Fla.) 26 (2014) 992–1005, https://doi.org/10.1002/adma.201304138.
[29] B. Anasori, M.R. Lukatskaya, Y. Gogotsi, Nat. Rev. Mater. 2 (2017) 16098, https://doi.org/10.1038/natrevmats.2016.98.
[30] W. Lian, Y. Mai, C. Liu, L. Zhang, S. Li, X. Jie, Ceram. Int. 44 (2018) 20154–20162, https://doi.org/10.1016/j.ceramint.2018.07.309.
[31] D. Zhang, M. Ashton, A. Ostadhossein, A.C.T. van Duin, R.G. Hennig, S.B. Sinnott, ACS Appl. Mater. Interf. 9 (2017) 34467–34479, https://doi.org/10.1021/acsami.7b09895.
[32] J. Yang, B. Chen, H. Song, H. Tang, C. Li, Crystal Res. Technol. 49 (2014) 926–932,

https://doi.org/10.1002/crat.201400268.
[33] X. Zhang, M. Xue, X. Yang, Z. Wang, G. Luo, Z. Huang, X. Sui, C. Li, RSC Adv. 5 (2015) 2762–2767, https://doi.org/10.1039/C4RA13800G.
[34] M. Xue, Z. Wang, F. Yuan, X. Zhang, W. Wei, H. Tang, C. Li, RSC Adv. 7 (2017) 4312–4319, https://doi.org/10.1039/C6RA27653A.
[35] Y. Liu, X. Zhang, S. Dong, Z. Ye, Y. Wei, J. Mater. Sci. 52 (2017) 2200–2209, https://doi.org/10.1007/s10853-016-0509-0.
[36] H. Zhang, L. Wang, Q. Chen, P. Li, A. Zhou, X. Cao, Q. Hu, Mater. Des. 92 (2016) 682–689, https://doi.org/10.1016/j.matdes.2015.12.084.
[37] Y.J. Mai, Y.G. Li, S.L. Li, L.Y. Zhang, C.S. Liu, X.H. Jie, J. Alloys Comp. 770 (2019) 1–5, https://doi.org/10.1016/j.jallcom.2018.08.100.
[38] R.M. Ronchi, J.T. Arantes, S.F. Santos, Ceram. Int. 45 (2019) 18167–18188, https://doi.org/10.1016/j.ceramint.2019.06.114.
[39] A. Rosenkranz, P.G. Grützmacher, R. Espinoza, V.M. Fuenzalida, E. Blanco, N. Escalona, F.J. Gracia, R. Villarroel, L. Guo, R. Kang, F. Mücklich, S. Suarez, Z. Zhang, Appl. Surf. Sci. 494 (2019) 13–21, https://doi.org/10.1016/j.apsusc.2019.07.171.
[40] Y. Guo, X. Zhou, D. Wang, X. Xu, Q. Xu, Langmuir ACS J. Surf. Colloids 35 (2019) 14481–14485, https://doi.org/10.1021/acs.langmuir.9b02619.
[41] X. Yin, J. Jin, X. Chen, A. Rosenkranz, J. Luo, ACS App. Mater. Interf. 11 (2019) 32569–32576, https://doi.org/10.1021/acsami.9b11449.
[42] X. Yin, J. Jin, X. Chen, A. Rosenkranz, J. Luo, Adv. Eng. Mater. (2020), https://doi.org/10.1002/adem.201901369.
[43] ISO, 104:2015-09 Rolling bearings - Thrust bearings - Boundary dimensions, general plan.
[44] M. Hu, T. Hu, Z. Li, Y. Yang, R. Cheng, J. Yang, C. Cui, X. Wang, ACS Nano 12 (2018) 3578–3586, https://doi.org/10.1021/acsnano.8b00676.
[45] T. Hu, J. Wang, H. Zhang, Z. Li, M. Hu, X. Wang, Phys. Chem. Chem. Phys. PCCP 17 (2015) 9997–10003, https://doi.org/10.1039/C4CP05666C.
[46] X. Zhang, Y. Liu, S. Dong, Z. Ye, Y. Guo, Ceram. Int. 43 (2017) 11065–11070, https://doi.org/10.1016/j.ceramint.2017.05.151.
[47] J. Halim, K.M. Cook, M. Naguib, P. Eklund, Y. Gogotsi, J. Rosen, M.W. Barsoum, Appl. Surf. Sci. 362 (2016) 406–417, https://doi.org/10.1016/j.apsusc.2015.11.089.
[48] J.F. Moulder, W.F. Stickle, P.E. Sobol, K.D. Bomben, Handbook of X-ray photoelectron spectroscopy: A reference book of standard spectra for identification of XPS data, Perkin-Elmer, Minsesota, op. 1992.
[49] M.V. Kuznetsov, S.V. Borisov, O.P. Shepatkovskii, Y.G. Veksler, V.L. Kozhevnikov, J. Synch. Investig. 3 (2009) 331–337, https://doi.org/10.1134/S102745100903001X.
[50] M.C. Biesinger, L.W.M. Lau, A.R. Gerson, R.S.C. Smart, Appl. Surf. Sci. 257 (2010) 887–898, https://doi.org/10.1016/j.apsusc.2010.07.086.
[51] T. Tanuma, H. Okamoto, K. Ohnishi, S. Morikawa, T. Suzuki, Catal. Lett. 136 (2010) 77–82, https://doi.org/10.1007/s10562-009-0197-3.
[52] I.P. Asanov, V.M. Paasonen, L.N. Mazalov, A.S. Nazarov, J. Struct. Chem. 39 (1998) 928–932, https://doi.org/10.1007/BF02903607.
[53] A.A. Galuska, J.C. Uht, N. Marquez, J. Vacuum Sci. Technol. A: Vacuum Surf., Films 6 (1988) 110–122, https://doi.org/10.1116/1.574992.
[54] J. Kröner, S. Kursawe, Y. Musayev, S. Tremmel, AMM 856 (2016) 143–150, https://doi.org/10.4028/www.scientific.net/AMM.856.143.
[55] J. Kröner, S. Tremmel, S. Kursawe, Y. Musayev, T. Hosenfeldt, S. Wartzack, AMM 805 (2015) 147–153, https://doi.org/10.4028/www.scientific.net/AMM.805.147.